ACADEMIC PRESS

Available online at www.sciencedirect.com

SCIENCE DIRECT®

Journal of Solid State Chemistry 175 (2003) 39–45

JOURNAL OF SOLID STATE CHEMISTRY

http://elsevier.com/locate/jssc

# Crystal growth of a novel oxygen-deficient layered perovskite: $Ba_7Li_3Ru_4O_{20}$

Katharine E. Stitzer, William R. Gemmill, Mark D. Smith, and Hans-Conrad zur Loye*

*Department of Chemistry and Biochemistry, University of South Carolina, 631 Sumter St., Columbia, SC 29208, USA*

Received 7 November 2002; received in revised form 7 February 2003; accepted 13 February 2003

## Abstract

Single crystals of both $Ba_7Li_3Ru_4O_{20}$ and $Ba_4NaRu_3O_{12}$ were grown from reactive molten hydroxide fluxes. $Ba_7Li_3Ru_4O_{20}$ is a 7L-layer perovskite-related phase resulting from the stacking of six [$AO_3$] layers and one oxygen deficient [$AO_2$] layer, thereby creating $LiO_4$ tetrahedra in addition to the $LiO_6$ octahedra and face-sharing $Ru_2O_9$ bi-octahedra formed from the [$AO_3$] layers. The compound crystallizes in the space group $R\bar{3}m$ with $a = 5.7927(1)$ Å and $c = 50.336(2)$ Å, $Z = 3$. $Ba_4NaRu_3O_{12}$ crystallizes in the space group $P6_3mc$ with lattice parameters of $a = 5.8014(2)$ Å and $c = 19.2050(9)$ Å, $Z = 2$. $Ba_4NaRu_3O_{12}$ is identical to a previously reported neutron refinement structure. The magnetic properties of $Ba_7Li_3Ru_4O_{20}$ are also reported.

*Keywords:* $Ba_7Li_3Ru_4O_{20}$; $Ba_4NaRu_3O_{12}$; Oxide materials; Oxygen deficient; Crystal growth; Single-crystal structure determination; Magnetic properties

## 1. Introduction

In the field of solid-state chemistry, the perovskite family of oxides is perhaps the most studied group of oxides known. What has generated and sustained the interest in this fascinating family of oxides is the large and ever surprising variety of properties exhibited, as well as the extensive compositional flexibility [1] that enables this structure to accommodate almost every element in the periodic table. Many investigations, consequently, have focused on the study of specific properties including complex magnetic phenomena and electrical properties such as superconductivity, ferroelectricity and ionic conductivity, to mention a few, while others explored the synthesis of new compositions or the stabilization of metals in heretofore unreported or unusual oxidation states [1–5].

In its ideal form, the structure of the cubic $ABO_3$ perovskite can be described as consisting of corner-sharing $BO_6$ octahedra with the A cation occupying the 12-fold coordination site formed in the middle of a cube of eight such octahedra, while the 2H-hexagonal variant consists of infinite chains of face-sharing octahedra that are separated by chains of the A cation. Both the cubic and the hexagonal perovskite structure can be generated from the stacking of close-packed [$AO_3$] layers, as shown in Fig. 1a, and the subsequent filling of the generated octahedral sites by the B cation, where an ABC-type stacking results in the cubic and an AB stacking results in the hexagonal (2H) perovskite structure [6,7]. In addition to the cubic and hexagonal $ABO_3$ structures, there exist a variety of intergrowth structures that combine the AB and ABC stacking sequences. Thus, both the triple, $A_3BB'_2O_9$, and the quadruple perovskite, $A_4BB'_3O_{12}$, contain both corner-sharing octahedra, consistent with ABC stacking, and face-sharing bi-octahedra, consistent with AB stacking.

Further structural variety in the extended perovskite family of oxides arises from the incorporation of oxygen deficient [$AO_2$] layers, as shown in Fig. 1b [8]. The stacking of such an oxygen deficient [$AO_2$] layer with [$AO_3$] layers generates a layer of tetrahedral instead of octahedral sites. $Ba_4Ca_{0.9}Mn_{3.1}O_{11.3}$ is an example of a structure in which the presence of an [$AO_2$] layer creates such a layer of tetrahedral sites; these tetrahedra vertices connect to octahedra above and below the plane, generating a layered, oxygen-deficient structure [9].

For the past 10 years, our group has explored the single-crystal growth of perovskite-related oxides from

---

*Corresponding author. Fax: +803-777-8508.

*E-mail address:* zurloye@sc.edu (H.-C. zur Loye).

0022-4596/03/$ - see front matter

doi:10.1016/S0022-4596(03)00112-9

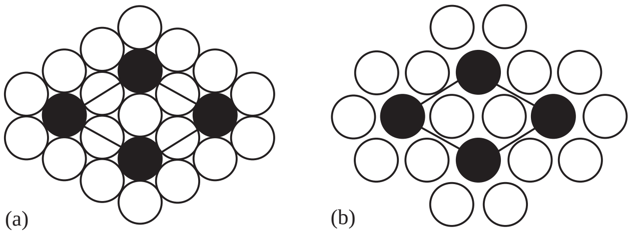

Fig. 1. Schematic of (a) [$AO_3$] and (b) [$AO_2$] layers with A (●) cations and O (○) anions.

high-temperature solutions [4,10–18]. This well-established method [19] is particularly applicable to oxides, as exemplified by the numerous published compositions containing elements from nearly every section of the periodic table in a wide range of oxidation states [19]. Oxide crystals have been grown from a variety of different high-temperature solutions, including alkali and alkaline earth carbonates, halides, peroxides, super oxides, and hydroxides [11,12,20–24]. Of all these diverse solvent systems, the hydroxide melts have proven to be particularly advantageous for obtaining single crystals containing elements in unusually high oxidation states, as exemplified by systems such as Ni(IV) in $Ba_6Ni_5O_{15}$ [25], Rh(V) in $Sr_3NaRhO_6$ [5], and Os(VII) in $Ba_2NaOsO_6$ [4].

More recently, we have focused our attention on ruthenium-containing oxides and on establishing the conditions by which high-quality single crystals can be grown from high-temperature solutions. Ruthenium is a particularly interesting metal in oxide chemistry as it has been incorporated into numerous perovskite-related structures, including simple, double, triple and quadruple perovskite structures [26–31]. In these systems ruthenium can be found in oxidation states of +4, +5, +6, and +7 [29,30,32] which often cause interesting magnetic interactions due to spin coupling between different ruthenium cations [27,31,33].

In this paper, we present a new oxygen-deficient perovskite, $Ba_7Li_3Ru_4O_{20}$, containing $LiO_4$ tetrahedral sites due to the presence of [$AO_2$] layers. In addition, we present the crystal growth conditions for preparing single crystals of a ruthenium quadruple perovskite, $Ba_4NaRu_3O_{12}$, whose structure was previously reported by Battle and co-workers as a polycrystalline sample [31].

## 2. Experimental

### 2.1. Crystal growth

$RuO_2$ (synthesized from heating Ru powder (Engelhard, 99.5%) in air for 24 h) (0.1336 g, 1.00 mmol), $Ba(OH)_2 \cdot 8H_2O$ (1.0315 g, 3.27 mmol; Fisher, ACS reagent), $LiOH \cdot H_2O$ (5.83 g, 139 mmol; Alfa Aesar, ACS reagent) with KOH (3.97 g, 70.8 mmol; Fisher, ACS reagent) for $Ba_7Li_3Ru_4O_{20}$ and NaOH (11.63 g, 291 mmol; Fisher, ACS reagent) for $Ba_4NaRu_3O_{12}$, were placed in an alumina crucible. The filled crucibles were placed into a box furnace with no lid in the case of $Ba_7Li_3Ru_4O_{20}$ and with a loose fitting alumina lid for the preparation of $Ba_4NaRu_3O_{12}$, and heated to the reaction temperature of 700°C at 600°C/h. The crucibles were held at temperature for 12 h and then slowly cooled to 600°C at 15°C/h followed by cooling to room temperature by turning off the furnace. The flux was dissolved with methanol in the case of the lithium preparation and water for the sodium preparation. Flux dissolution was also aided by the use of sonication followed by manual isolation of the crystals.

### 2.2. Microscopy

Environmental scanning electron micrographs (ESEM) of several single crystals were obtained using a Philips XL 30 ESEM instrument utilized in the environmental mode. ESEM images of representative crystals of $Ba_7Li_3Ru_4O_{20}$ and $Ba_4NaRu_3O_{12}$ are shown in Fig. 2. EDS also verified the presence of barium, ruthenium, and oxygen in all samples, and the presence of sodium in $Ba_4NaRu_3O_{12}$. Furthermore, within the detection limits of the instrument, no other extraneous elements were detected.

### 2.3. Magnetic susceptibility

The magnetic susceptibility of $Ba_7Li_3Ru_4O_{20}$ was measured using a Quantum Design MPMS XL SQUID magnetometer. For the magnetic measurements, loose crystals of the ruthenate were placed into a gelatin capsule, which was placed inside a plastic straw. Samples were measured under both zero-field-cooled (ZFC) and field-cooled (FC) conditions. In either case the magnetization was measured in the temperature range of 2–400 K. Susceptibility measurements were carried out in applied fields of 0.5, 5, and 20 kG. The very small diamagnetic contribution of the gelatin capsule containing the sample had a negligible contribution to the overall magnetization, which was dominated by the sample signal.

### 2.4. Data collection

For the structure determination of $Ba_7Li_3Ru_4O_{20}$ and $Ba_4NaRu_3O_{12}$, a black prismatic crystal and a black hexagonal needle, respectively, were mounted onto the end of thin glass fibers. X-ray intensity data were measured at 293 K on a Bruker SMART APEX CCD-based diffractometer system (Mo$K\alpha$ radiation, $\lambda = 0.71073$ Å) [34].

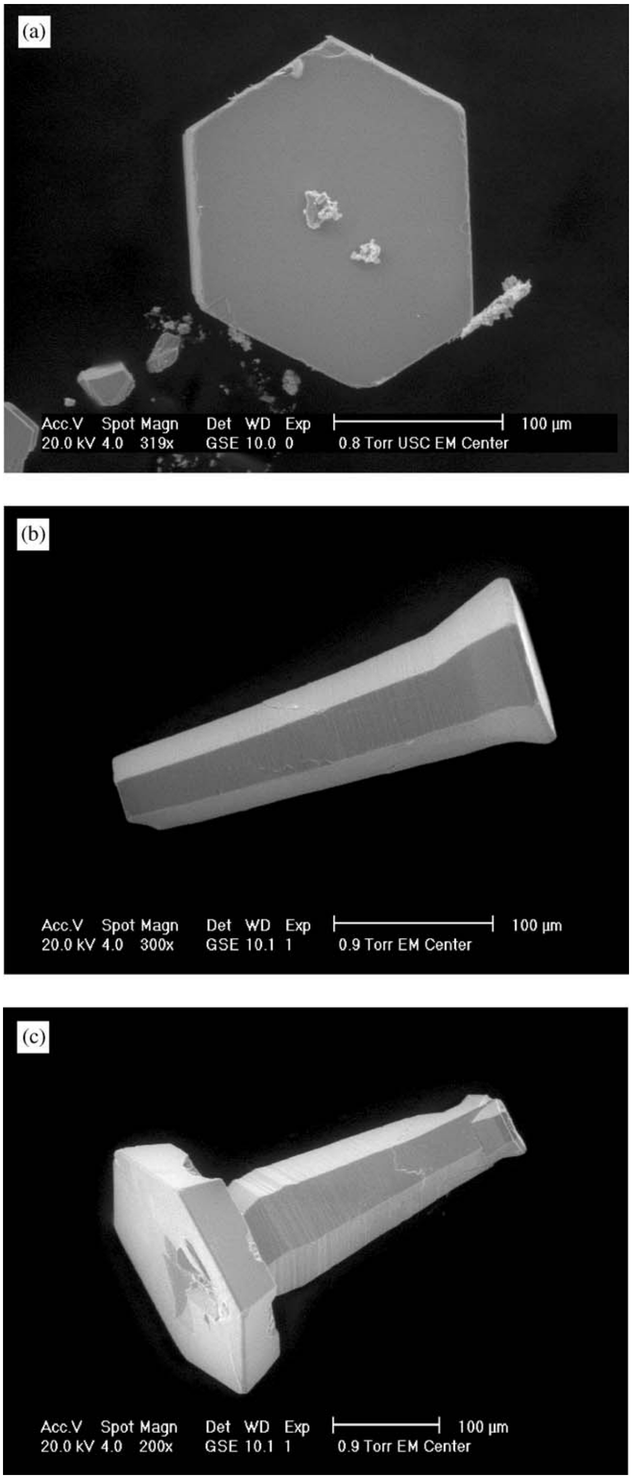

Fig. 2. ESEM images of flux grown crystals of $Ba_7Li_3Ru_4O_{20}$ (a) and $Ba_4NaRu_3O_{12}$ (b and c).

For $Ba_7Li_3Ru_4O_{20}$, preliminary scans to check crystal quality and unit-cell parameters indicated a rhombohedral system with $a \sim 5.8$ Å and $c \sim 50.3$ Å. Several crystals were checked to verify the unusual cell dimensions; none indicated a different cell. The data collection for both compounds provided 99.7% coverage of reciprocal space to $2\theta_{max} = 80.5°$ ($R_{int} = 0.0304$, average redundancy = 5.75) and 99.0% coverage of reciprocal space to $2\theta_{max} = 75.6°$ ($R_{int} = 0.0326$, average redundancy = 10.8) for $Ba_7Li_3Ru_4O_{20}$ and $Ba_4NaRu_3O_{12}$, respectively. The raw data frames were integrated with the Bruker SAINT + program [34], which also applied corrections for Lorentz and polarization effects. The final unit-cell parameters were based on the least-squares refinement of 5182 reflections for $Ba_7Li_3Ru_4O_{20}$ and 5495 reflections for $Ba_4NaRu_3O_{12}$ with $I > 5\sigma(I)$ from the data set. Analysis of each data set showed negligible crystal decay during data collection. An empirical absorption correction based on the multiple measurement of equivalent reflections was applied with the program SADABS [34].

For $Ba_7Li_3Ru_4O_{20}$, systematic absences in the intensity data clearly ruled out a $c$-glide operation, leaving the space groups $R3$, $R\bar{3}$, $R32$, $R3m$ and $R\bar{3}m$, the latter of which was eventually confirmed. For $Ba_4NaRu_3O_{12}$, systematic absences in the intensity data indicated the space groups $P6_3mc$ and $P6_3/mmc$; the structure was subsequently solved in the noncentrosymmetric space group $P6_3mc$. The structures of both compounds were solved by a combination of direct methods and difference Fourier syntheses, and refined by full-matrix least-squares against $F^2$, using the SHELXTL software package [35]. For $Ba_7Li_3Ru_4O_{20}$, all metal atoms are located on three-fold axes. The oxygen atoms are located on mirror planes. Oxygen $O_4$ at the apex of the $Li(1)O_4$ tetrahedron occupies a split position around a three-fold axis, distributed over the three sites with occupancy 1/3. Initial refinement of $O_4$ on the three-fold axis resulted in an aberrantly large disk-shaped ellipsoid. Eventually, all atoms were refined with anisotropic displacement parameters. At convergence, the largest difference peak and hole were $+3.87$ and $-2.84\,e^-/Å^3$, located near $Ba_3$ and $Ba_4$, respectively. Relevant crystallographic information for $Ba_7Li_3Ru_4O_{20}$ is gathered in Table 1, while the atomic positions are located in Table 2.

In the case of $Ba_4NaRu_3O_{12}$, subsequent examination of the structure confirmed the space group choice of $P6_3mc$. $Ba_4NaRu_3O_{12}$ is isostructural with the previously published sample, which was refined against powder neutron data [31]. Near the end of the present refinement, the value of the absolute structure (Flack) parameter was 0.44(4), indicating racemic (inversion) twinning. This was accounted for using the TWIN $-1\,0\,0/0\,-1\,0/0\,0\,-1$ command in SHELX, with the Flack parameter as the twin proportion. Eventually, all atoms were refined with anisotropic displacement parameters. The final difference map featured maxima of $+5.70$ and $-3.05\,e^-/Å^3$, located $<1$ Å from Ru1 and Ba3, respectively. Relevant crystallographic information for $Ba_4NaRu_3O_{12}$ is compiled in Table 3, and the atomic positions are located in Table 4.

Table 1
Crystallographic data and structure refinement for $Ba_7Li_3Ru_4O_{20}$

| | | |
|---|---|---|
| Empirical formula | $Ba_7Li_3Ru_4O_{20}$ | |
| Formula weight | 1706.48 | |
| Temperature | 293(2) K | |
| Wavelength | 0.71073 Å | |
| Crystal system | Trigonal | |
| Space group | $R\bar{3}m$ | |
| Unit-cell dimensions | $a = 5.7927(1)$ Å | $\alpha = 90°$ |
| | $b = 5.7927(1)$ Å | $\beta = 90°$ |
| | $c = 50.336(2)$ Å | $\gamma = 120°$ |
| Volume | 1462.77(6) $Å^3$ | |
| $Z$ | 3 | |
| Density (calculated) | 5.812 $mg/m^3$ | |
| Absorption coefficient | 16.975 $mm^{-1}$ | |
| Reflections collected | 7216 | |
| Independent reflections | 1252 [$R(int) = 0.0304$] | |
| Absorption correction | Semi-empirical from equivalents | |
| Data/restraints/parameters | 1252/0/48 | |
| Goodness-of-fit on $F^2$ | 1.247 | |
| Final R indices [$I > 2\sigma(I)$] | $R_1 = 0.0320$, $wR_2 = 0.0791$ | |
| R indices (all data) | $R_1 = 0.0345$, $wR_2 = 0.0805$ | |
| Extinction coefficient | 0.00075(4) | |
| Largest diff. peak and hole | 3.872 and −2.841 e $Å^{-3}$ | |

Table 2
Atomic coordinates and equivalent isotropic parameters for $Ba_7Li_3Ru_4O_{20}$

| Atom | Occupancy | $x$ | $y$ | $z$ | $U_{eq}$ ($Å^2$) |
|---|---|---|---|---|---|
| Ba(1) | 1 | 0 | 0 | 0 | 0.050(1) |
| Ba(2) | 1 | 0 | 0 | 0.1917(1) | 0.013(1) |
| Ba(3) | 1 | 0 | 0 | 0.2783(1) | 0.011(1) |
| Ba(4) | 1 | 0 | 0 | 0.4307(1) | 0.011(1) |
| Ru(1) | 1 | 0 | 0 | 0.0690(1) | 0.008(1) |
| Ru(2) | 1 | 0 | 0 | 0.1236(1) | 0.008(1) |
| Li(1) | 1 | 0 | 0 | 0.3657(3) | 0.012(2) |
| Li(2) | 1 | 0 | 0 | 1/2 | 0.022(4) |
| O(1) | 1 | 0.3018(5) | 0.1509(3) | 0.0962(1) | 0.011(1) |
| O(2) | 1 | 0.1591(3) | 0.3181(5) | 0.1427(1) | 0.013(1) |
| O(3) | 1 | 0.1589(3) | 0.3179(6) | 0.0490(1) | 0.015(1) |
| O(4) | 1/3 | 0.6143(14) | 0.3857(14) | 0.0034(2) | 0.036(3) |

Table 3
Crystallographic data and structure refinement for $Ba_4NaRu_3O_{12}$

| | | |
|---|---|---|
| Empirical formula | $Ba_4NaRu_3O_{12}$ | |
| Formula weight | 1067.65 | |
| Temperature | 293(2) K | |
| Wavelength | 0.71073 Å | |
| Crystal system | Hexagonal | |
| Space group | $P6_3mc$ | |
| Unit-cell dimensions | $a = 5.8014(2)$ Å | $\alpha = 90°$ |
| | $b = 5.8014(2)$ Å | $\beta = 90°$ |
| | $c = 19.2050(9)$ Å | $\gamma = 120°$ |
| Volume | 559.77(4) $Å^3$ | |
| $Z$ | 2 | |
| Density (calculated) | 6.334 $mg/m^3$ | |
| Absorption coefficient | 17.874 $mm^{-1}$ | |
| Reflections collected | 7149 | |
| Independent reflections | 942 [$R(int) = 0.0326$] | |
| Absorption correction | Semi-empirical from equivalents | |
| Data/restraints/parameters | 942/1/51 | |
| Goodness-of-fit on $F^2$ | 1.236 | |
| Final R indices [$I > 2\sigma(I)$] | $R_1 = 0.0320$, $wR_2 = 0.0791$ | |
| R indices (all data) | $R_1 = 0.0345$, $wR_2 = 0.0805$ | |
| Extinction coefficient | 0.0031(4) | |
| Largest diff. peak and hole | 5.699 and −3.051 e $Å^{-3}$ | |

Table 4
Atomic coordinates and equivalent isotropic parameters for $Ba_4NaRu_3O_{12}$

| Atom | $x$ | $y$ | $z$ | $U_{eq}$ ($Å^2$) |
|---|---|---|---|---|
| Ba(1) | 0 | 0 | 0.1173(1) | 0.010(1) |
| Ba(2) | 1/3 | 2/3 | 0.3715(1) | 0.011(1) |
| Ba(3) | 2/3 | 1/3 | 0.4947(1) | 0.012(1) |
| Ba(4) | 1/3 | 2/3 | 0.7471(1) | 0.009(1) |
| Ru(1) | 0 | 0 | 0.2990(1) | 0.007(1) |
| Ru(2) | 0 | 0 | 0.4371(1) | 0.008(1) |
| Ru(3) | 1/3 | 2/3 | 0.1810(1) | 0.006(1) |
| Na(1) | 1/3 | 2/3 | 0.5608(5) | 0.011(1) |
| O(1) | 0.1621(6) | 0.3241(12) | 0.2449(4) | 0.012(1) |
| O(2) | 0.3012(10) | 0.1506(5) | 0.3652(4) | 0.010(1) |
| O(3) | 0.1583(6) | 0.3166(12) | 0.4887(4) | 0.015(1) |
| O(4) | 0.5146(5) | 0.4854(5) | 0.6277(3) | 0.009(1) |

## 3. Results and discussion

### 3.1. Crystal structures

Small black hexagonal plates of $Ba_7Li_3Ru_4O_{20}$ and needles of $Ba_4NaRu_3O_{12}$, were isolated from molten hydroxide fluxes, where the flux acted both as the melt and reactant. The crystals measured, on average, 0.1–0.3 mm in length. ESEM images of both ruthenates are shown in Fig. 2. $Ba_7Li_3Ru_4O_{20}$, shown in Fig. 2a, exhibits a more hexagonal plate-like morphology, in comparison to $Ba_4NaRu_3O_{12}$, shown in Figs. 2b and c, which has a more rod-like morphology. Interestingly, crystals of $Ba_4NaRu_3O_{12}$ appear to start as a plate and then elongate into a rod, where the crystals resemble nails on the micro-scale. EDS analysis verified the presence of barium, ruthenium, and oxygen for both samples and sodium for $Ba_4NaRu_3O_{12}$; however, lithium was not observed for $Ba_7Li_3Ru_4O_{20}$ as it is below the detection limit of the instrument. In both cases, no extraneous elements were identified within the detection limits of the instrument.

An approximate [110] view of $Ba_7Li_3Ru_4O_{20}$ is shown in Fig. 3. The structure consists of two layers of $Ru_2O_9$ bi-octahedra that are connected to one another via corner-shared octahedra. Above and below this structure block are layers of $LiO_4$ tetrahedra that vertex share to the bi-octahedra. Three such tetrahedra–bi-octahedra–octahedra–bi-octahedra–tetrahedra blocks are arranged in an ABC repeat, creating the long (50.3 Å) $c$-axis.

The repeat unit of the structure closely approximates a triple perovskite structure in which the repeat is two face-sharing octahedra followed by a vertex-shared octahedra; however, in $Ba_7Li_3Ru_4O_{20}$, due to the presence of an oxygen deficient [$AO_2$] layer, a tetrahedral site takes the place of the expected octahedral site. This similarity is highlighted in Fig. 4, which shows the triple perovskite structure next to one of the repeat blocks of the $Ba_7Li_3Ru_4O_{20}$ structure. In terms of layer stacking, the $Ba_7Li_3Ru_4O_{20}$ structure is best described as a 7L-layer sequence along the *c*-direction with a hexagonal stacking of [$AO_3$] layers (h), cubic stacking of [$AO_3$] layers (c), and cubic stacking of [$AO_2$] layers (c′) according to the sequence $(chcchcc')_3$.

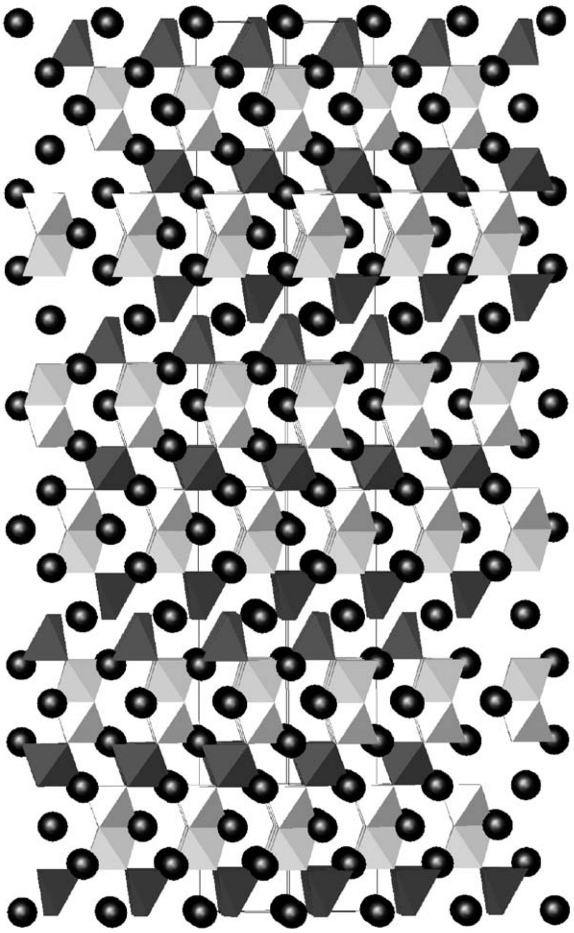

Fig. 3. Approximate [110] view of the structure of $Ba_7Li_3Ru_4O_{20}$ consisting of light gray $Ru_2O_9$ face-sharing bi-octahedra and dark gray $LiO_4$ tetrahedra and $LiO_6$ octahedra. Barium cations are shown as black spheres.

The presence of oxygen-deficient layers in perovskites is not new; however, this structure, nonetheless, is the first of its kind, and represents a clear expansion of the known perovskite crystal chemistry. Furthermore, it suggests that the pursuit of other oxygen-deficient structures related to the triple and quadruple perovskites should be a worthwhile undertaking.

Using the crystal growth conditions described for this compound, it is possible to force high oxidation states onto the metals in the crystals; however, there are chemical limitations as to what the highest achievable oxidation state is for any particular metal. Consequently, in structures where the elemental stoichiometry would force the metal to take on too-high an oxidation state, one often observes oxygen deficient layers that charge compensate and enable the metal to remain in a slightly lower oxidation state. The presence of oxygen-deficient layers, such as [$AO_2$] layers, creates tetrahedral sites, as previously described.

Interestingly, if $Ba_7Li_3Ru_4O_{20}$ were a fully oxidized compound, the composition would be $Ba_7Li_3Ru_4O_{21}$, resulting in three Ru(VI) and one Ru(VII) and an average oxidation state of $Ru+6.25$, which would be quite unusual for a ruthenium oxide prepared under ambient pressure conditions. Hence, perhaps by chemical necessity, the presence of the [$AO_2$] layer eliminates this problem, and lowers the overall oxidation state to $+5.75$.

Selected interatomic distances for $Ba_7Li_3Ru_4O_{20}$ are compiled in Table 5. For $Ba_7Li_3Ru_4O_{20}$, the Li–O distances in the tetrahedra of 1.939(7) and 1.877(18) Å

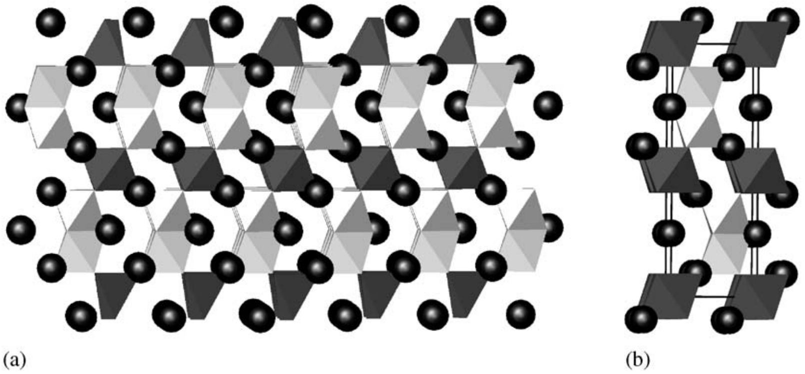

Fig. 4. The structural similarity between (a) $Ba_7Li_3Ru_4O_{20}$ and the triple perovskite (b) $A_3A'B_2O_9$ is readily apparent from the [110] views. The insertion of an [$AO_2$] layer creates the tetrahedral sites in $Ba_7Li_3Ru_4O_{20}$ instead of the corresponding octahedral sites in the triple perovskite.

Table 5
Selected interatomic distances for $Ba_7Li_3Ru_4O_{20}$ and $Ba_4NaRu_3O_{12}$

| Atom–atom | Distance (Å) | | Atom–atom | Distance (Å) | |
|---|---|---|---|---|---|
| $Ba_7Li_3Ru_4O_{12}$ | | | | | |
| Ru(1)–O(1) | 2.043(3) | (×3) | Li(1)–O(3) | 1.939(7) | (×3) |
| Ru(1)–O(3) | 1.885(3) | (×3) | Li(1)–O(4) | 1.877(18) | (×3) |
| Ru(2)–O(1) | 2.045(3) | (×3) | Li(2)–O(2) | 2.125(3) | (×6) |
| Ru(2)–O(2) | 1.863(3) | (×3) | | | |
| Ru(1)–Ru(2) | 2.747(7) | (×1) | | | |
| $Ba_4NaRu_3O_{12}$ | | | | | |
| Ru(1)–O(1) | 1.931(6) | (×3) | Ru(3)–O(4) | 1.839(5) | (×3) |
| Ru(1)–O(2) | 1.977(6) | (×3) | Ru(1)–Ru(2) | 2.653(13) | (×1) |
| Ru(2)–O(2) | 2.048(7) | (×3) | Na(1)–O(3) | 2.238(9) | (×3) |
| Ru(2)–O(3) | 1.875(7) | (×3) | Na(1)–O(4) | 2.229(7) | (×3) |
| Ru(3)–O(1) | 2.114(6) | (×3) | | | |

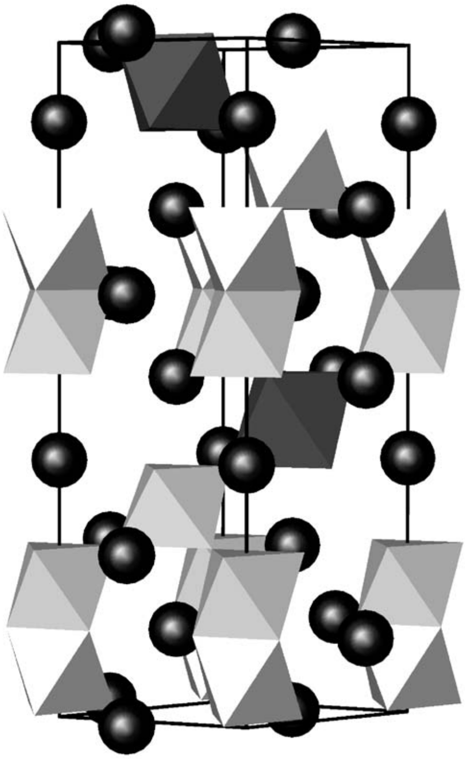

Fig. 5. Approximate [110] view of the structure of $Ba_4NaRu_3O_{12}$ consisting of light gray $Ru_2O_9$ face-sharing bi-octahedra and octahedra singles and dark gray $NaO_6$ octahedra. Barium cations are shown as black spheres.

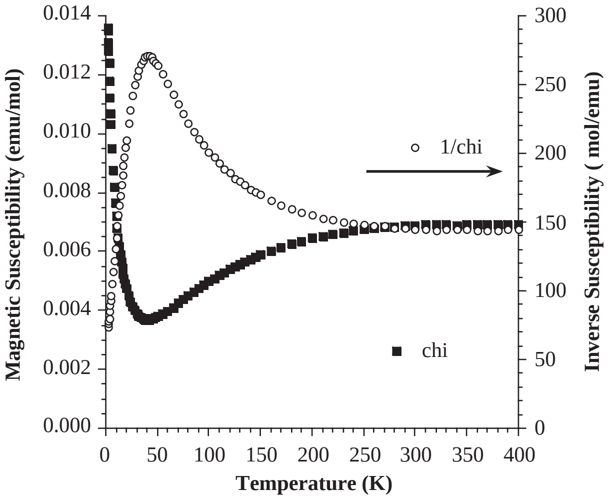

Fig. 6. Temperature dependence of the ZFC magnetic susceptibility (■) and inverse susceptibility (○) of $Ba_7Li_3Ru_4O_{20}$ at an applied field of 20 kG.

are comparable with those found in the literature [36]. Likewise, the Li–O distance in the octahedra of 2.125(3) Å is consistent with octahedral distances found in similar perovskite-related phases [4,37]. The grouping of three short Ru–O distances at 1.863(3) and 1.885(3) Å and three long at 2.043(3) and 2.045(3) Å within the $Ru_2O_9$ bi-octahedra is typical for the bi-octahedra in triple perovskites. By analogy with ruthenium triple perovskites, the short Ru–O distances of ~1.87 Å and the long Ru–Ru separation of 2.747(7) Å in $Ba_7Li_3Ru_4O_{20}$, correlates with the average oxidation state of ruthenium in the complex [37], and is consistent with an oxidation state between +5.5 and +6. By charge balance, $Ba_7Li_3Ru_4O_{20}$ consists of three Ru(VI) and one Ru(V) yielding an average oxidation state of Ru+5.75.

The crystal structure of $Ba_4NaRu_3O_{12}$ is shown in Fig. 5 and is consistent with the one reported by Battle and co-workers [31]. The structure consists of a repeat of face-sharing $Ru_2O_9$ bi-octahedra followed by vertex-shared $RuO_6$ octahedra and $NaO_6$ octahedra. The layer stacking can be described as $(hccc)_2$ where (h) is the hexagonal stacking of $[AO_3]$ layers and (c) is the cubic stacking of $[AO_3]$ layers.

The interatomic distances of $Ba_4NaRu_3O_{12}$ are consistent with those previously reported [31]. It is again possible to use the structural information for the ruthenium bi-octahedra to make assignments of the average ruthenium oxidation state. In this structure, the short Ru–O distances of 1.931(6) and 1.875(7) Å and the Ru–Ru distance of 2.653(13) Å are consistent with the expected average oxidation state of Ru+5.

### 3.2. *Magnetism*

The temperature dependence of the magnetic susceptibility for $Ba_7Li_3Ru_4O_{20}$ in an applied field of 20 kG is shown in Fig. 6. The susceptibility decreases to a minimum at ~40 K followed by an increase. The ZFC and FC data completely overlay at all temperatures, and thus the FC data have been omitted for clarity. It can be observed from the plot of the inverse susceptibility, also shown in Fig. 6, that even at temperatures up to 400 K, the material does not follow Curie–Weiss-type behavior.

Moreover, because of the mixed site occupancy, we were unable to model the magnetism using an isolated dimer model, as the three Ru(VI) and one Ru(V) cations are disordered over two crystallographic sites. The shape of the susceptibility curve, however, is very similar to those observed for compounds, $Ba_3CaRu_2O_9$ [33] and $Ba_5Ru_2O_{10}$ [38], in which the $Ru_2O_9$ bi-octahedra were modeled magnetically as antiferromagnetically coupled "isolated dimers". Consequently, it seems reasonable to suggest that the dimers are coupling antiferromagnetically in this system as well.

## 4. Conclusion

A novel layered ruthenate was grown from a molten hydroxide flux. The structure consists of a 7L-layer stacking sequence of $(chcchcc')_3$ where (c′) is an oxygen-deficient layer creating tetrahedral sites within the structure. The Ru–O and Ru–Ru interatomic distances within the $Ru_2O_9$ bi-octahedra are consistent with an average oxidation state of Ru + 5.75. The crystal growth of $Ba_4NaRu_3O_{12}$ is also reported.

## Acknowledgments

Financial support from the National Science Foundation through Grant DMR:0134156 is gratefully acknowledged.

**Supporting information available:**

Further details of the crystal structure investigation can be obtained from the Fachinformationszentrum Karlsruhe, 76344 Eggenstein-Leopoldshafen, Germany, (fax: (49) 7247-808-666; email: mailto:crysdata@fiz-karlsruhe.de) on quoting the depository number CSD-412836 and CSD-412837.

## References

[1] K.E. Stitzer, J. Darriet, H.-C. zur Loye, Curr. Opin. Solid State Mater. Sci. 5 (2001) 535.
[2] L.F. Schneemeyer, J.K. Thomas, T. Siegrist, B. Batlogg, L.W. Rupp, R.L. Opila, R.J. Cava, D.W. Murphy, Nature 335 (1988) 421.
[3] K.R. Kendall, C. Navas, J.K. Thomas, H.-C. zur Loye, Solid State Ionics 82 (1995) 215.
[4] K.E. Stitzer, M.D. Smith, H.-C. zur Loye, Solid State Sci. 4 (2002) 311.
[5] B.A. Reisner, A.M. Stacy, J. Am. Chem. Soc. 120 (1998) 9682.
[6] J.J. Lander, Acta Crystallogr. 4 (1951) 148.
[7] A.F. Wells, Structural Inorganic Chemistry, Clarendon Press, New York, 1984.
[8] J. Darriet, M.A. Subramanian, J. Mater. Chem. 5 (1995) 543.
[9] W. Schuddinck, G. Van Tendeloo, M. Hervieu, N. Floros, B. Raveau, Mater. Res. Bull. 36 (2001) 2689.
[10] J.B. Claridge, R.C. Layland, R.D. Adams, H.-C. zur Loye, Z. Anorg Allg. Chem. 623 (1997) 1131.
[11] J.B. Claridge, R.C. Layland, W.H. Henley, H.-C. zur Loye, Chem. Mater. 11 (1999) 1376.
[12] W.H. Henley, J.B. Claridge, P.L. Smallwood, H.-C. zur Loye, J. Cryst. Growth 204 (1999) 122.
[13] M.D. Smith, H.-C. zur Loye, Acta Crystallogr. C 57 (2001) 337.
[14] K.E. Stitzer, A. El Abed, J. Darriet, H.-C. zur Loye, J. Am. Chem. Soc. 123 (2001) 8790.
[15] K.E. Stitzer, M.D. Smith, J. Darriet, H.-C. zur Loye, Chem. Commun. 1680 (2001).
[16] H.-C. zur Loye, R.C. Layland, M.D. Smith, J.B. Claridge, J. Cryst. Growth 211 (2000) 452.
[17] H.-C. zur Loye, K.E. Stitzer, M.D. Smith, A. El Abed, J. Darriet, Inorg. Chem. 40 (2001) 5152.
[18] M. Zakhour-Nakhl, J.B. Claridge, J. Darriet, F. Weill, H.-C. zur Loye, J.M. Perez-Mato, J. Am. Chem. Soc. 122 (2000) 1618.
[19] D. Elwell, H.J. Scheel, Crystal Growth from High-Temperature Solutions, Academic Press, New York, 1975.
[20] S. Frenzen, Hk. Müller-Buschbaum, Z. Naturforsch. 50b (1995) 581.
[21] M. Neubacher, Hk. Müller-Buschbaum, Z. Anorg. Allg. Chem. 607 (1992) 124.
[22] M.D. Smith, J.K. Stalick, H.-C. zur Loye, Chem. Mater. 11 (1999) 2984.
[23] G. Wehrum, R. Hoppe, Z. Anorg. Allg. Chem. 617 (1992) 45.
[24] K.E. Stitzer, M.D. Smith, H.-C. zur Loye, J. Alloys Compd. 338 (2002) 104.
[25] J.A. Campá, E. Gutiérrez-Puebla, M.A. Monge, I. Rasines, C. Ruíz-Valero, J. Solid State Chem. 108 (1994) 230.
[26] J.J. Randal, R. Ward, J. Am. Chem. Soc. 81 (1959) 2629.
[27] S.H. Kim, P.D. Battle, J. Solid State Chem. 114 (1995) 174.
[28] P.D. Battle, C.W. Jones, J. Solid State Chem. 78 (1989) 108.
[29] P. Lightfoot, P.D. Battle, J. Solid State Chem. 89 (1990) 174.
[30] Y. Doi, M. Wakeshima, Y. Hinatsu, A. Tobo, K. Ohoyama, Y. Yamaguchi, J. Mater. Chem. 11 (2001) 3135.
[31] P.D. Battle, S.H. Kim, A.V. Powell, J. Solid State Chem. 101 (1992) 161.
[32] H. Samata, A. Mishiro, S. Sawada, Y. Nagata, T. Uchida, M. Kai, M. Ohtsuka, M. Der Lan, J. Phys. Chem. Solids 59 (1998) 1445.
[33] J. Darriet, M. Drillion, G. Villeneuve, P. Hagenmuller, J. Solid State Chem. 19 (1976) 213.
[34] SMART Version 5.624, SAINT + Version 6.02a and SADABS. Bruker Analytical X-ray Systems, Inc., Madison, WI, USA, 1998.
[35] G.M. Sheldrick, SHELXTL Version 5.1, Bruker Analytical X-ray Systems, Inc., Madison, WI, USA, 1997.
[36] T.R. Jensen, P. Norby, J.C. Hanson, O. Simonsen, E.M. Skou, P.C. Stein, H.A. Boye, J. Mater. Chem. 8 (1998) 969.
[37] K.E. Stitzer, M.D. Smith, W.R. Gemmill, H.-C. zur Loye, J. Am. Chem. Soc. 124 (2002) 13877.
[38] F. Grasset, M. Zakhour, J. Darriet, J. Alloys Compd. 287 (1999) 25.